Micro-mechanics based pressure dependent failure model for highly cross-linked epoxy resins

J Chevalier, X P Morelle, C Bailly, P P Camanho, T Pardoen, F Lani

"Micro-mechanics based pressure dependent failure model for highly cross-linked epoxy resins"

Chevalier, Jérémy ; Morelle, Xavier ; Bailly, Christian ;
Camanho, P.P. ; Pardoen, Thomas ; Lani, Frédéric

Abstract

A new fracture criterion for semi brittle epoxy materials is developed, expressed in terms of the attainment of a local critical value of the maximum principal stress at the tip of small internal defects. The criterion is assessed on the highly cross-linked structural epoxy resin RTM6 used as matrix in fiber reinforced composites. Based on finite element simulations of unit cells, the local stress field at the tip of ellipsoidal defects is related to the macroscopic loading. The overall fracture stress levels measured on uniaxial tension and compression specimens are used to identify the two parameters of the failure criterion which involves the characteristic aspect ratio of the microdefects and the critical maximum principal tensile stress. An upper bound to the size of the microdefect is determined based on fracture mechanics arguments. The fracture criterion accurately predicts the fracture for a wide range of stress triaxialities from overall compression conditions to tensile wi...

Document type : *Article de périodique (Journal article)*

Micro-mechanics based pressure dependent failure model for highly cross-linked epoxy resins

J. Chevalier[a,*], X.P. Morelle[a], C. Bailly[b], P.P. Camanho[c], T. Pardoen[a], F. Lani[a]

[a] *Institute of Mechanics, Materials and Civil Engineering (IMMC), Université catholique de Louvain, Place Sainte-Barbe, n2, L05.02.02, 1348 Louvain-la-Neuve, Belgium*

[b] *Institute of Condensed Matter and Nanosciences (IMCN), Université catholique de Louvain, Place L. Pasteur, n1, L04.01.01, 1348 Louvain-la-Neuve, Belgium*

[c] *aDEMec, Faculdade de Engenharia, Universidade do Porto, Rua Dr. Roberto Frias, s/n, 4200-465 Porto, Portugal*

Abstract

A new fracture criterion for semi brittle epoxy materials is developed, expressed in terms of the attainment of a local critical value of the maximum principal stress at the tip of small internal defects. The criterion is assessed on the highly cross-linked structural epoxy resin RTM6 used as matrix in fiber reinforced composites. The criterion relies on Based on finite element simulations of unit cells, the local stress field at the tip of ellipsoidal defects is related to the macroscopic loading. The overall fracture stress levels measured on uniaxial tension and compression specimens are used to identify the two parameters of the failure criterion which involves the characteristic aspect ratio of the microdefects and the critical maximum principal tensile stress. An upper bound to the size of the microdefect is determined based on fracture mechanics arguments. The fracture criterion accurately predicts the fracture for a wide range of stress triaxialities from overall compression conditions to tensile with additional hydrostatic component related to different notched configurations.

Keywords: Failure criterion, maximum principal stress, pressure dependence, finite element method, unreinforced resin

1. Introduction

The proper modeling and prediction of the mechanical response of fiber reinforced polymers (FRP) used in high-performance structural applications require an accurate and physically sound description of the deformation and failure behaviour of the matrix. On the one hand, in many occasions, the composite is considered linear elastic and a variety of failure criteria are used to predict the load carrying capability of components. Advanced criteria [1, 2] already include well identified matrix-dominated failure modes, incorporating some (limited) non-linearity in the behaviour of the latter [2], based on rough estimations of the stress and strain partitioning between the matrix and the fibres. As in several conditions the resin is the locus of first damage [3, 4], the assessment of these engineering criteria against detailed micromechanical models of plies and even laminates requires properly identified and accurate constitutive models and failure criteria for the resin itself, in order to predict the failure locus, which is an image of the dependence of the deformation and failure of the composite on the stress/strain level and stress-triaxiality in the constituents of the plies. On the other hand, in certain shear-dominated conditions, the resin dictates even more the response of the component as its ductility plays a more prominent role. A typical example is the bias-loading of biaxial laminates where significant non-linear deformation can be achieved before the occurence of delamination [5]. Beside a good geometrical description of the meso and micro-architectures, the modeling of this configuration obviously requires a very good knowledge of the deformation and failure behaviour of the resin (as well as of the

*Corresponding author
Email address: jeremy.chevalier@uclouvain.be (J. Chevalier)

Nomenclature

FE	Finite Element
RVE	Representative Volume Element
MPS	Maximum Principal Stress
CTOD, δ	Crack Tip Opening Displacement
$\sigma^{\text{local}}_{\text{princ,max}}$	maximum principal stress reached in the vicinity of the small internal microstructural defects
A_r	aspect ratio of the spheroidal defects
σ^{∞}_{ij}	stress tensor at RVE scale
σ_c	local critical principal stress at which failure is initiated
$\bar{\varepsilon}^p$	Equivalent plastic strain
σ_y	yield strength
ΔMPS	$\text{MPS}_{tension} - \text{MPS}_{compression}$
ε_f	equivalent fracture strain
G_{Ic}	mode I critical energy release rate
δ_c	critical CTOD

interface). Note that the non-linear behaviour of the resin is expected to be of increasing influence as the strain-rate decreases, e.g. such as in creep, and the temperature increases [6].

In this work, as a major ingredient to subsequent multi-scale analyses, the failure of the aerospace grade structural epoxy resin RTM6 is investigated based on a micromechanical approach, considering the non-linear deformation behaviour identified by Morelle et al. [7] as input data.

At first sight, the mechanical behaviour of the RTM6 epoxy resin is in line with the generally reported behavior of cross-linked thermoset polymers. It exhibits much larger ductility under compression than under tension in which fracture occurs after a few percents of elongation. However, when considering the mechanical behaviour of the RTM6 resin, two main issues arise. First, crazing is not observed. Crazing is known to lead to a brittle failure mechanism, initiated by the fracture of the remaining polymer fibrils within the crazes. The occurrence of crazes within epoxy resins has been reported only very few times and only in moderately cross-linked resins [8, 9]. To the authors' knowledge, the appearance of crazes has never been proved in highly cross-linked glassy polymers under tensile loadings, in the presence or not of stress concentrators such as notches or cracks [7, 10–12]. Therefore, the highly cross-linked network should prevent RTM6 from crazing, even under positive triaxialities, hence disabling the usual origin for explaining a brittle failure mechanism in glassy polymers. Second, brittle fracture is observed in compression tests albeit at very large deformation above 50%, which can neither be explained by the appearance of crazes nor by the sole propagation of shear bands through the material. This aspect will be addressed in details in this paper. As crazing involves the appearance of micro-voids, the negative triaxiality induced in the compression test clearly inhibits such a mechanism, while it is the main mechanism triggered under positive triaxialities [11]. Shear bands were not observed in uniaxial compression tests of RTM6 [7]. However, it is now admitted that shear-yielding can be a true intrinsic diffuse phenomenon, where softening is the result of the initiation, growth and coalescence of micro-shearing zones [13, 14]. Nevertheless, despite a significant ductility in compression, Morelle et al. [7] show that no plasticity-related progressive damage could be indirectly (through reduction of the modulus, or a non-saturation of back-stress upon unloading) or directly observed (e.g. particular features on fracture surfaces), and, as a consequence, failure could not be related to shear-induced plasticity or damage.

Some earlier studies in the literature had already been dedicated to the characterization of the visco-plasticity, creep, thermo-mechanical response and/or failure behaviour of the RTM6 [7, 15, 16], as well as of other epoxy resins

[12, 17–20], including moderately cross-linked resins.

In [7] Morelle et al. identified a series of empirical pressure or triaxiality-dependent macroscopic failure criteria, in-line with the works of Asp et al. [12] and Fiedler et al. [21]. The proposed criteria rely on the fact that micro-cavitation is responsible for failure and have shown a satisfactory predictive capability; however, the link with the micromechanics of cavitation was not done. Besides, several failure criteria for brittle and quasi-brittle solids have been identified beyond the particular case of glassy polymers. Most of them are based on the macroscopic properties of the material, such as the fracture toughness and the tensile strength [22], or on a characteristic length, which, often, does not possess a clear physical basis [23–26]. While these criteria have been shown to successfully predict the failure of many brittle materials, they are not able to unify the cases of brittle failure in both positive and negative triaxialities, and they are mainly motivated by the failure prediction in the presence of a macro-scale stress concentrator. An exception is the criterion developed by Leguillon [22] which was extended by Zhang and Li [27, 28] to un-notched specimens. None of these criteria provide a satisfying approach to explain the brittle failure both in compression and in tension of RTM6. The brittle and quasi-brittle fracture of materials under compression has been extensively studied by Wang and Shrive [29–31], mainly considering concrete and rocks. Their approach consists in considering that brittle fracture in compression is caused by surface separation involving a mode I cracking mechanism. They explained the appearance of this mode I cracking by the nucleation of cracks at the tip of pre-existing flaws, that is, flaws which are present in the material before the deformation process. The assumption is made that the defects can be modelled by ellipsoids. Our approach follows a similar line of thought.

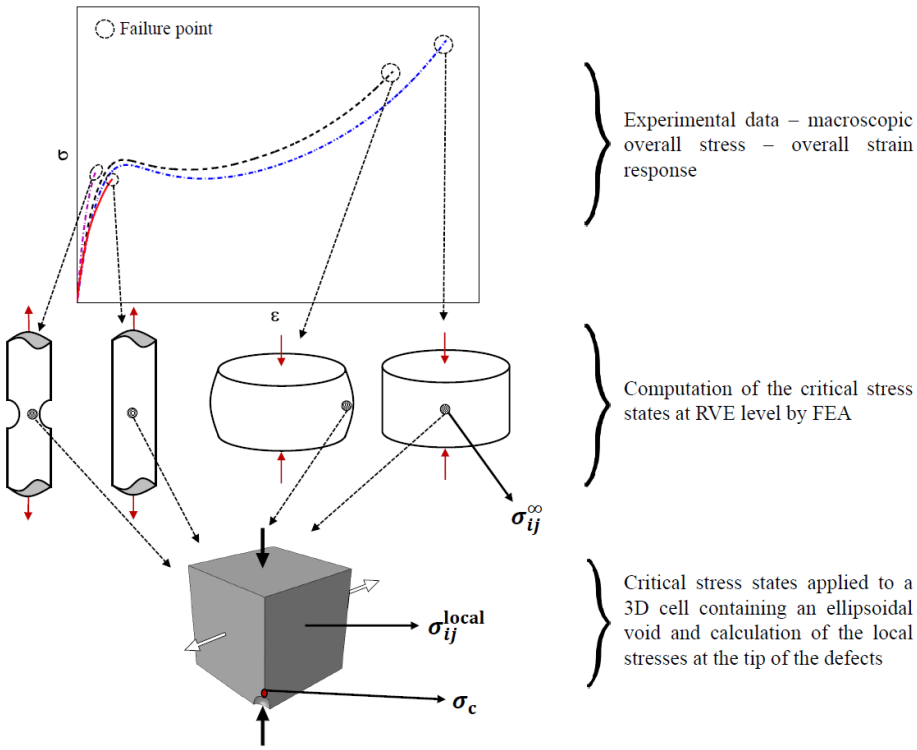

Figure 1: Schematic representation of the multiscale analysis; the black and white arrows respectively represent the compression and tensile loading applied to the FE unit cell, as to identify the maximum principal stress at the tip of the ellipsoidal void.

In this work, experimental results, involving pure compression and tensile tests on notched and unnotched specimens, are used to determine under different loading conditions the stress levels attained in RTM6, at the instant and location corresponding to the onset of fracture. The data reduction is based on Finite Element (FE) analyses of the macroscopic specimens. A brittle type fracture criterion based on the stress concentration effect of small internal microstructural defects is proposed as $\sigma^{\text{local}}_{\text{princ,max}}\left(A_r, \sigma^{\infty}_{ij}, \text{elasto-plastic properties}\right) = \sigma_c$, where A_r is the aspect ratio of the critical defects, σ^{∞}_{ij} is the stress tensor at RVE scale, the elasto-plastic properties involve the Young's modu-

lus, Poisson ratio and the hardening law $\sigma_y(\bar{\varepsilon}^p)$, σ_c is the local critical stress at which failure is initiated. This new criterion is initially based on the idea that the strength of the epoxy is mainly limited by the presence of pre-existing defects, as initially suggested by Griffith [32]. It provides a physical explanation of the pressure dependence of the failure stress and strain in highly cross-linked epoxy resins as it unifies the occurence of fracture under a wide range of stress triaxialities based on a single mechanism. The criterion relies on simulations at the microscopic scale on representative volume elements (RVE) of RTM6 containing a defect. The inverse identification on the experimental data allows the determination of the characteristics of the critical defects, while an upper limit of their size is defined thanks to fracture mechanics arguments. A schematic representation of the underlying logic of the multiscale analysis is shown in Fig. 1.

The outline of the paper is the following. The material and testing methods are presented in section 2 and details on the FE simulations made are given in section 3. Section 4 is dedicated to the experimental results, the identification of the model parameters based on these results and on the validation of the proposed failure criterion. Conclusions are given in section 5.

2. Materials, processing and testing methods

2.1. Material

The monocomponent HexFlow RTM6 epoxy resin from Hexcel has been developed for application as matrix in carbon fiber reinforced composites in the aeronautic and space structural components. The material is supplied as a premixed system composed of tetra-glycidylmethylenedianiline (TGMDA) epoxy polymer and of two amine curing-agents M-DEA and M-DIPA. The RTM6 resin has a high glass transition temperature Tg = 220°C, extracted from differential scanning calorimetry (DSC), which guarantees good thermal stability for applications up to 180°C.

2.2. Processing

First, the supplied mixture was poured into pre-heated release-agent coated moulds. The uncured resin was then degassed during 75min at 90°C under vacuum. The curing phase was divided in two cycles. (1) The mixture was heated from 90°C to 130°C at a heating rate of 2°C/min, followed by a low-temperature curing cycle at 130°C during 3 hours. This step is necessary to avoid local over-heating in the slabs. (2) Then, a three hour post-curing step was imposed at a higher temperature (180°C), with a heating ramp equal to 2°C/min. The samples were cooled down to room temperature at a cooling rate of 10°C/min. The entire curing process leads to the attainment of a high cross-linking percentage (> 95%) as measured by alternating DSC.

2.3. Machining and mechanical testing

The cylindrical resin slabs were machined into small cylindrical specimens (diameter and height = 6mm) for uniaxial compression tests and into cylindrical dog bone specimens (diameter = 4mm and gauge length = 7mm) for uniaxial tensile tests. Notched specimens were also produced by classical machining of notches with different radii (1, 1.5, 2, 3 and 5 mm) into larger dog bone shape specimens (original diameter = 9mm, diameter at the notch tip = 4mm and gauge length = 50mm). The machining was performed very carefully and slowly enough to avoid heating as much as possible. Tensile and compression tests were carried out on a screw-driven universal testing machine (Zwick-Roell with a 250kN loading cell). All tests were performed at room temperature with a crosshead speed equal to 1mm/min. The axial displacement was measured based on a compliance corrected crosshead displacement method and the radial displacement in the notches was measured using a strictometer (LVDT). The friction and the induced barreling effect during the compression tests could be minimized thanks to PTFE films inserted between the platens of the testing machine and the specimens. Each test was repeated at least three times.

3. Finite element modeling

The FE simulations were carried out using the commercial code Abaqus [33]. The use of FE analyses was required by the need (i) to determine the overall critical stress state inside the macroscopic specimens at the onset of fracture and (ii) to compute the local stresses in the vicinity of a microdefect of aspect ratio A_r, assumed to be the initiator of the final fracture. To do so, the stress components calculated at the macroscopic scale and corresponding to the instant and location of fracture initiation are applied to a RVE containing a defect, as schematically represented in Fig. 1. The mechanical response of the resin is modeled by using, for the hardening law $\sigma_y(\bar{\varepsilon}^p)$, the macroscopic true stress - true plastic strain curve obtained by a uniaxial compression test at a strain rate of 1.6 $10^{-4}s^{-1}$. The hardening law was linearly extrapolated up to large equivalent true plastic strains with a slope equal to the one measured at the end of the experimental curve. The elastic response is linear and isotropic, characterized by Young's modulus $E = 3$GPa and Poisson ratio $\nu = 0.34$. In this first application of the new failure criterion, the material is assumed to be J2 elastic-plastic, strain rate independent and the pressure dependence on plastic yielding is neglected; but the present approach could certainly be refined to more complex constitutive models.

3.1. FE on macroscopic specimens

At the macroscopic scale, each mechanical test carried out on the resin specimens was simulated to accurately determine the stress states at the onset of failure at the RVE level. The simulations were made using the average test data from the 3 (or more) repetitions of the experiments. First-order and second-order axisymmetric quadrilateral elements were respectively used to simulate the tensile tests (on notched and unnotched specimens) and the compression tests.

3.2. FE on microscopic RVE

At the microscopic scale, in order to study the stress concentration effect of inherent defects in the material, simulations were carried out on a RVE, which contains a single defect. The defect is modeled as a spheroidal void with aspect ratio A_r, whose volume fraction is small enough not to influence the global mechanical response of the RVE. Furthermore, the volume fraction of the voids is considered to be low enough ($< 0.1\%$) to avoid inducing shear yielding in the ligaments between them [34] and such that it is not needed to simulate a vast population of defects to capture interaction effects. It is assumed that at each macroscopic point under stress σ_{ij}^{∞} there is a statistical distribution of defects such that there is always one defect oriented to maximize the local principal stress $\sigma_{\text{princ}}^{\text{local}}$ reached in its vicinity. This means that the defects are very small in such a way that a sufficiently large population of defects corresponds to a volume size over which the stress and strain are macroscopically constant or, at least, marginally varying. This question of physical scale separation will be addressed in section 4.4. The lower part of Fig. 1 shows the critical orientation of the defect with respect to the direction of the applied load (only one eighth of the geometry is modeled), as the white and the black arrows respectively illustrate the orientation of the tensile and compressive loads on the RVE. Second-order tetrahedral elements have been selected for the simulation of compression tests, in order to avoid hourglassing problems when large compressive strain is applied, while a structured mesh of first-order hexahedral elements was preferred around the defect in the case of tensile loadings. In both cases, the mesh is refined around the defect with a minimal element size of around 2% the length of the major axis of the spheroid. The physical scale separation applied in this case implies that only the relative size of the RVE and the elements with respect to the defect is meaningful. Overall, the RVE contains about 350000 elements.

4. Results and discussion

4.1. Experimental results

All uniaxial tensile tests carried out on the cylindrical dogbone specimens exhibit a brittle mode of fracture corresponding to a true tensile stress at failure equal to 105 ± 5[MPa] and a true strain at failure equal to 0.075 ± 0.0085. Fig. 2 shows reference true strain/true stress curves from these uniaxial tension tests on unnotched specimens and from the pure compression tests, emphasizing the much larger ductility of the RTM6 resin under compressive loading conditions. Fig. 2 also exhibits the effect of friction between the platens and the specimen by showing curves corresponding to tests performed with and without a lubricating PTFE film. The apparent hardening is more rapid

in the presence of friction while the strain to failure is significantly reduced. In both cases, the specimens exhibit the typical fracture surfaces associated with brittle failure modes. Fig. 3 shows scanning electron microscopy (SEM) micrographs of fracture surfaces obtained at the end of the compression tests. Fig. 3a provides a low magnification micrograph of a fragment resulting from the test, and the location of the micrographs given in Fig. 3b, 3c and 3d is indicated. The fragments either display flat mirror-like surfaces, a conical shape or a combination of both. A detailed explanation on each of the different features observed on the fracture surfaces represented in Fig. 3 is given in ref. [7]. The bottom line is that the patterns observed at the initiation of the cones (Fig. 3d) and on the mirror-like parts (Fig. 3b) support the idea of a fracture initiated because of a critical tensile stress. Indeed, as described by Hull [35], the appearance of river lines (see Fig. 3d) on the fracture surfaces suggests a mode I crack opening followed by a mode I/III propagation.

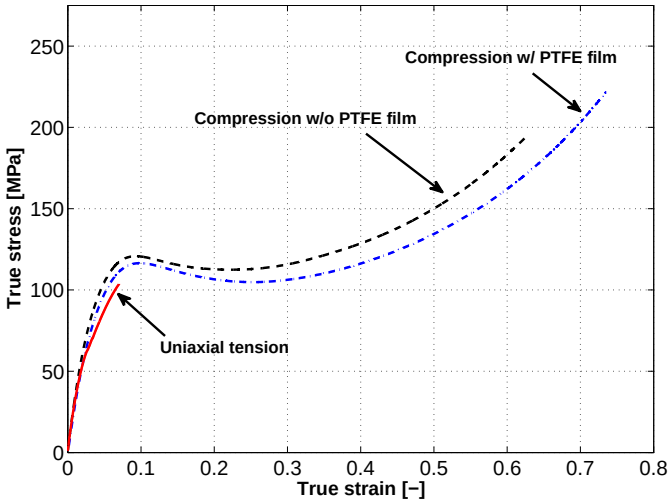

Figure 2: Representative true strain - true stress curves of RTM6 from the tension tests on unnotched specimens and from the compression tests with and without a PTFE film to reduce the friction with the platens.

Fig. 4a illustrates the effect of friction leading to the typical barrel shape near the end of the compression test. This barreling effect leads to the generation of significant tensile stresses along the surface of the specimen, which consequently accelerates the occurrence of the first crack in the material, explaining the lower failure stress and strain. The occurrence of this barreling effect when no PTFE is inserted between the platens and the specimens has been used as an additional stress state condition imposed to the RTM6 epoxy. Before modeling the compression test to extract the critical stress state at the RVE level, the coefficient of friction must be first determined to be included in the FE model in order to properly capture the contact conditions between the specimen and the platens. Images similar to the one shown in Fig. 4a were used to extract coordinates of several points on the specimen surfaces and to reproduce the profile of the deformed surfaces. The friction coefficient was identified by reverse analysis: the value $\mu = 0.07$ was found to minimize the distance between the simulated and the measured profile of the deformed edge, as shown in Fig. 4b.

The FE analyses carried out in order to quantify the magnitude of the tensile stresses induced by the barreling effect, using the identified coefficient of friction, showed that these stresses, around 30 to 35MPa, were actually much lower than the stress leading to failure in the tensile tests. This local tensile stress certainly contributes to reaching the failure condition but cannot account alone for the initiation of cracking. It is worth noting that the radial cracks formed on the barreled edge of the specimens (see top of Fig. 5) do not propagate through the entire specimen. The reason is that these cracks rapidly enter into a region where closing forces inhibit their propagation. Thus, in most cases, instead of directly leading to the failure of the material, the cracks are deviated, leading to a peeling phenomenon (see lower part of Fig. 5). The peeling of the material at the edges leads to a decrease of the cross section area and, consequently, to a significant increase of the compressive stress in the uncracked regions of the specimen, inducing its final failure.

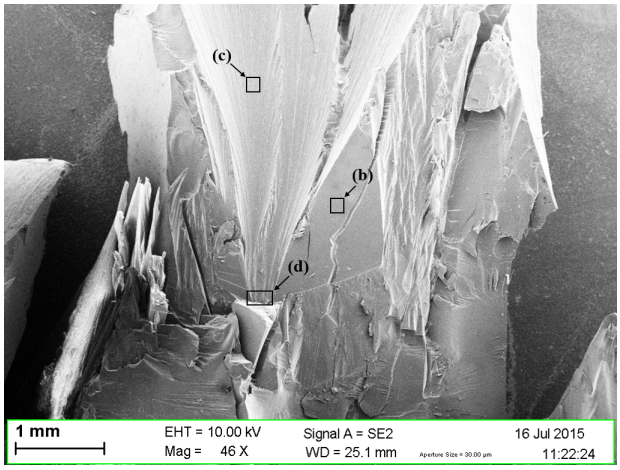

(a)

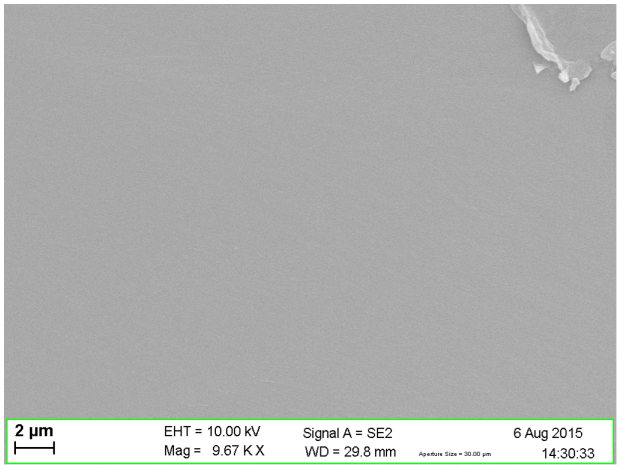

(b)

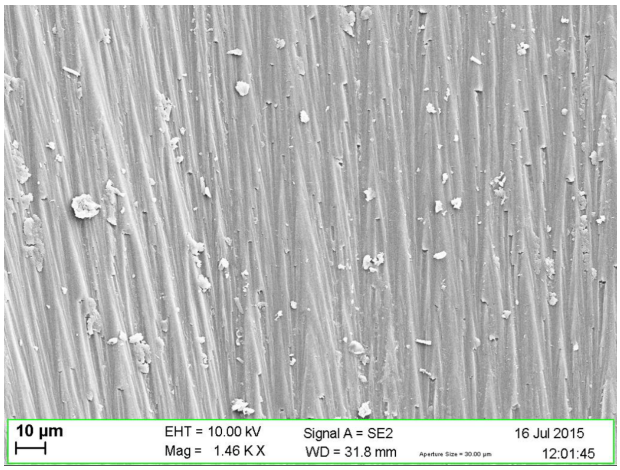

(c)

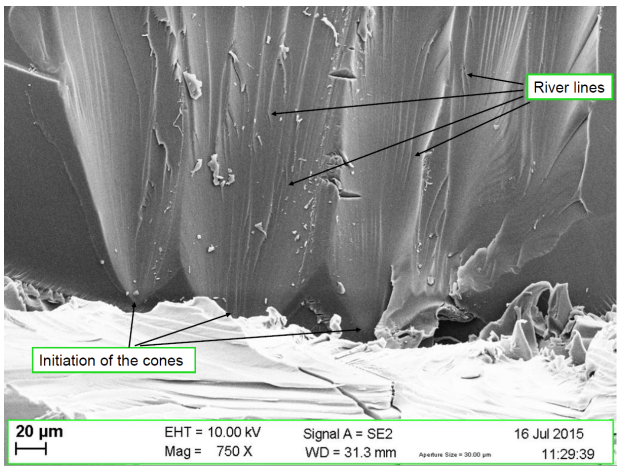

(d)

Figure 3: SEM micrographs of RTM6 fracture surfaces following a pure compression test from [7] : a) overview of a fragment, b) mirror-like fracture surface, c) characteristic triangular pattern on a cone-like part, d) initiation of the cones showing a river-lines pattern.

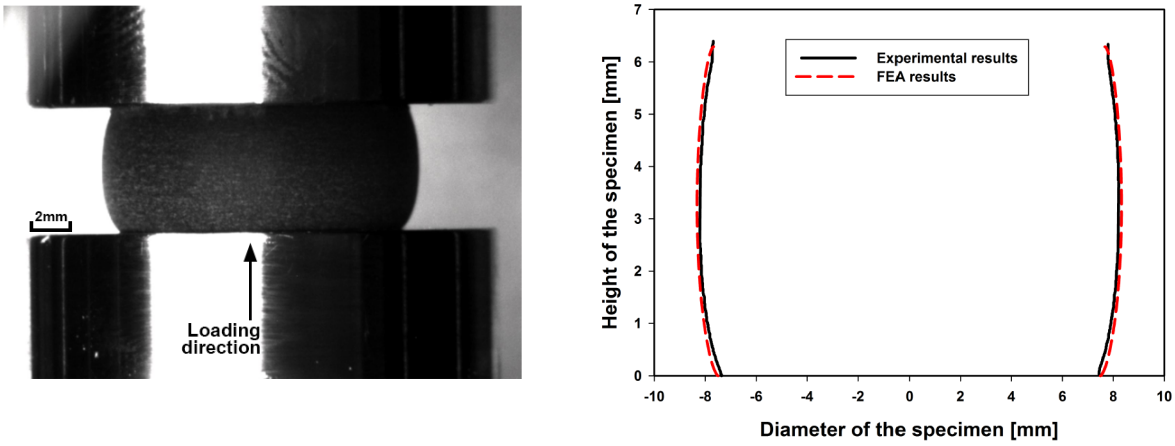

(a) (b)

Figure 4: a) Illustration of the barreling effect when no PTFE film is used ; b) comparison between the shape of the deformed surface of the specimen under pure compression between the experimental test with barreling and the corresponding FE simulation with $\mu = 0.07$.

The fact that the tensile stresses induced by the barreling only act as an accelerating factor is supported by the fact that similar brittle fracture is observed even when friction is minimized owing to the PTFE films, that is, when no barreling develops. In this case, the overall maximum principal stress (MPS) is almost zero and cannot be the direct cause of the failure of the material. The similar aspect of the fracture patterns with and without friction clearly suggests that the failure mechanism is the same in both cases, but that cracking is only activated earlier because of the existence of hoop tensile stresses when barreling takes place. As expected, the appearance of earlier cracks on the surface of the specimens with no barreling was rarely observed. This macroscopic analysis of the compression tests constitutes one of the key motivations for looking at a fracture criterion based on a population of pre-existing microdefects. Indeed, only pre-existing defects could lead to local tensile stresses large enough to allow the initiation of cracking.

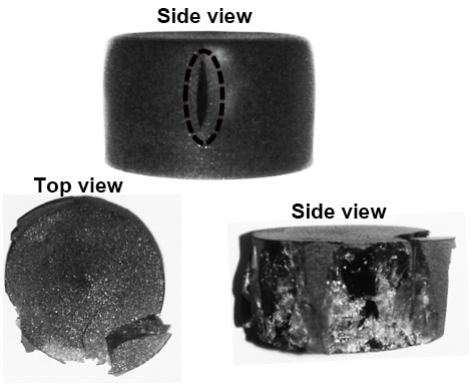

Figure 5: Images showing the formation of cracks on the barreled surface (top) and the initiation of the peeling phenomenon (bottom).

Tensile tests on notched specimens were carried out in order to determine the sensitivity of the fracture strain of RTM6 to the notch radius (1, 1.5, 2, 3 and 5 mm). Fig. 6a shows reference force-displacement curves from the tensile tests performed on each specimen geometry. The results were used to compute the stress states right before

failure occurs based on FE simulations of the tests. Fig. 6b shows the MPS variation near the notch along the ligament perpendicular to the loading direction, for each notch radius, at the load corresponding to fracture. The MPS attained in the notched specimens is very similar and close to the one reached in uniaxial tensile tests on unnotched specimens, which is equal to the true tensile stress at failure. Hence, from a macroscopic view point, it is a first good approximation to assume that the fracture of the RTM6 specimens is controlled by a critical overall MPS value if under overall tensile conditions. However, such a criterion alone will obviously not work for predicting fracture in pure compression specimens.

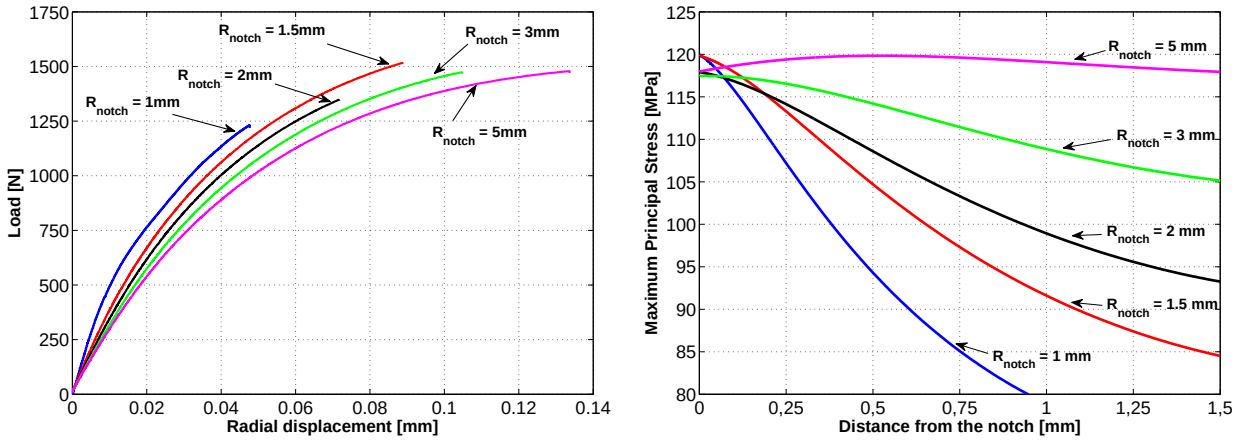

(a) (b)

Figure 6: a) Reference load-displacement curves of the tensile tests on notched specimens; b) variation of the maximum principal stress as a function of the distance to the notch root right at failure, computed by FE analyses.

4.2. Identification of the failure parameters at microscale on 3D unit cells FE calculations

The brittle type fracture observed both in tension and compression, despite the much larger strain and absolute stress to failure under compression, indicating a similar physical mechanism. In order to encompass both tensile and compression loading conditions, the hypothesis is made that the fracture of RTM6 is initiated when a critical principal stress is attained locally near characteristic internal defects of the material. Each defect acts as a stress concentrator leading, even under compression, to local tensile conditions. Hobbiebrunken et al. [36] already suggested a weakening effect of the intrinsic defects in the RTM6 resin, as they showed an increase of strength in tension when the specimen size was reduced to fibers. More interestingly, they also showed a drastic increase of the scatter in the strength of the fibers. Such an increase of the scatter points towards the presence of a population of internal weakening microdefects in the specimens.

The microdefect is modeled as a spheroidal void. At each macroscopic point which describes the response of a RVE of the microstructure, it is assumed that there is statistically always a defect that is positioned, with respect to the applied load, as to maximize the principal stress in its vicinity. In order to identify the parameters entering the fracture criterion, the first step is to find out if there is an aspect ratio A_r of the microdefect that could potentially lead to the same local MPS when fracture occurs both in uniaxial compression and uniaxial tension. This would, from a phenomenological viewpoint, provide a strong justification for the validity of the underlying model assumptions. The experimental loading conditions corresponding to the regions of the specimen where fracture initiates (i.e. in the zone with the largest MPS at macroscale) were applied to the 3D unit cell represented at the bottom of Fig. 1, following the direction of the black and white arrows for the uniaxial compression and tension, respectively. This stress-strain history is computed by the FE analysis of the specimen. For the uniaxial compression tests, the final stress state applied to the 3D unit cell corresponds to the instant of the first crack appearance. While the volume of the defect was kept constant, the aspect ratio A_r was varied. The local MPS in the finite element unit cell was then extracted for each different case. The aspect ratio A_r of the critical defect was subsequently found by simply calculating the difference

between the MPS attained in tension and in compression (= ΔMPS), at the corresponding A_r. The best aspect ratio corresponds to ΔMPS = 0. Fig. 7a shows the variation of ΔMPS with respect to A_r of the defect. An aspect ratio A_r of the critical defect between 0.26 and 0.27 provides the best predictive capability for the proposed fracture criterion.

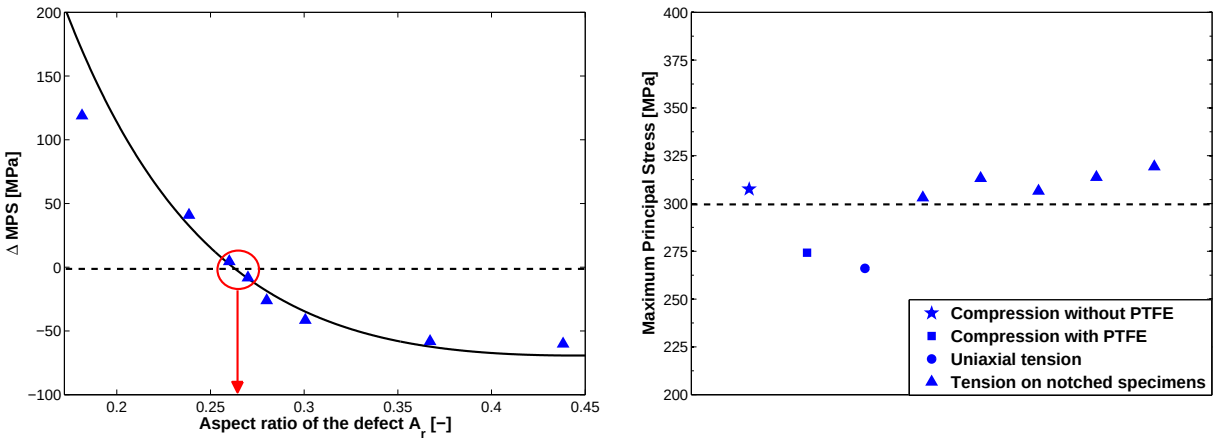

(a) (b)

Figure 7: a) Variation of ΔMPS (local MPS in tension - local MPS in compression) with respect to the aspect ratio of the defect. The black curve represents an exponential evolution of ΔMPS fitting the numerical data ; b) MPS reached at the tip of the defect in all cases, the dashed line corresponds to MPS = 300 [MPa].

The results obtained on the notched specimens and on the barreled specimens can be used to validate the new fracture criterion using the identified value of A_r. Fig. 7b shows the MPS attained in the vicinity of the microscale defect in the 3D FE simulation for all the cases (uniaxial tension, all notch radii and compression with and without PTFE), using $A_r = 0.27$. While there is some scatter among the data, all the results nicely group around MPS = 300MPa. Moreover, higher MPS are reached in the specimens where the stress state is not homogeneous during the test (i.e. compression with barreling and tension on notched specimens). The variability in the results shown in Fig. 7b could actually find an explanation in a simple statistical effect. Indeed, the area in the specimen where the stress state is critical enough to induce failure is much smaller in the notched specimens and in the barreled specimens (at least when the first crack appears). Therefore, the probability of the presence of the assumed critical defect, that is, sharp enough and properly oriented, in a smaller volume is lower. As a consequence, in average, the failure is probably caused by a defect which is slightly less critical than the one identified thanks to the pure uniaxial tensile and compression tests, leading to higher MPS when the same critical defect is used in the FE analyses. It is also worth remembering that the failure criterion is identified here based on a very simple constitutive model not accounting for pressure dependence.

4.3. Validation of the model

Fig. 8 shows the statistical variation of the near defect MPS at failure if it is identified for each test replicate on the notched specimens and not on the average value. The dashed line is for MPS = 300MPa, highlighting the fact that 300MPa lies in the standard deviation intervals for each notch radius, except for $R = 5$mm. The practical validation of the accuracy of the predictions obtained with the new criterion consists in calculating the fracture strain ε_f based on a local critical MPS of 300MPa in the vicinity of a microdefect with $A_r = 0.27$ would predict for each specimen. Fig. 9 shows ε_f for each stress triaxiality and the corresponding error bars. All predictions are well within the intervals delimited by the experimental error bars, establishing the predictive character of the criterion in this range of loading conditions.

The identified value of the critical MPS equal to 300MPa can be qualitatively justified in the following way. It has been shown by Zhurkov et al. [37] that the fracture of cross-linked polymers is caused by the rupture of primary

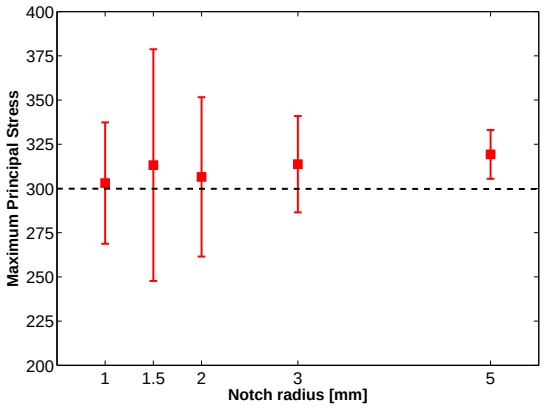

Figure 8: Maximum principal stress at the edge of the microscale defect for each notch radius for a macroscopic loading corresponding to fracture, and illustration of the experimental variability of the tensile tests on the notched specimens over that maximum principal stress; the dashed line shows the 300MPa mark.

covalent bonds in the material. A brittle fracture process has been observed in all the tests that were made in this work (as well as in [21]), which suggests that it must indeed be the case for all the tested stress triaxialities. Moreover, as theoretically explained by Lake and Thomas [38], in order to break a polymer chain, the entire chain must be stressed at the level of the strength of its weakest covalent bond. Therefore, there is every reason to believe that in all the tests made, the chains in the vicinity of the small-scale defect are progressively stretched during the loading until they undergo a mean stress level of about 300MPa. When such a stress is reached, the chains break and a crack is initiated in the resin. Applying the study of the theoretical strength of isotropic solids made by Kelly [39], approximately equal to $E/10$ for epoxy resins [11], with E being the Young's modulus, to the RTM6 resin ($E = 3000$MPa) gives $\sigma_{\text{f,theo}} \cong 3000\text{MPa}/10 = 300\text{MPa}$. It is worth noting that the critical MPS values which exceed 300MPa in Fig. 7b are only the consequence of the statistical effect described at the end of section 4.2. Moreover, it is one of the shortcomings related to the need to determine a precise and single value for the aspect ratio of the critical defects in order to eventually model and predict the failure of highly cross-linked epoxy resins. Hence, a single value for A_r will unavoidably lead to higher values than the theoretical strength of epoxy resins, but Fig. 8 shows that using MPS=300MPa for all the tested stress triaxialities still gives very accurate predictions of the fracture strain.

4.4. Physical size of the microscale defects

The open remaining question is about the physical interpretation of the criterion and, more specifically, about the nature and the size of the assumed microdefects. At this stage and without more in depth characterization efforts, only preliminary arguments can be formulated on this issue to legitimate the approach. Two approaches can be used to give an estimation of the defects size. The most straightforward approach relies on the analysis of fractographic images and to directly measure the size of the defect at the position of fracture initiation. However, such defects could hardly be found on these micrographs. This is an indication of the expected very small size of the defects responsible for cracking initiation. The second approach relies on fracture mechanics and is therefore based on the hypothesis that the mechanism of crack propagation in a pre-cracked specimen is identical to the one identified in this study. First, an upper bound of the defect size can be given by considering the concept of crack tip opening displacement (CTOD or δ) defined in the context of fracture mechanics. A critical value δ_c can be estimated thanks to [40]:

$$\delta_c = d\frac{G_{\text{Ic}}}{\sigma_{\text{y}}} \tag{1}$$

with $G_{\text{Ic}} = 200\text{J/m}^2$ and $\sigma_{\text{y}} = 110$MPa for RTM6 [6, 7]. Following the Irwin plastic zone correction for plane stress, $d = 4/\pi$ in the limit of small-scale yielding [40]. Hence, the critical opening δ_c of a macroscopic precrack is around 1

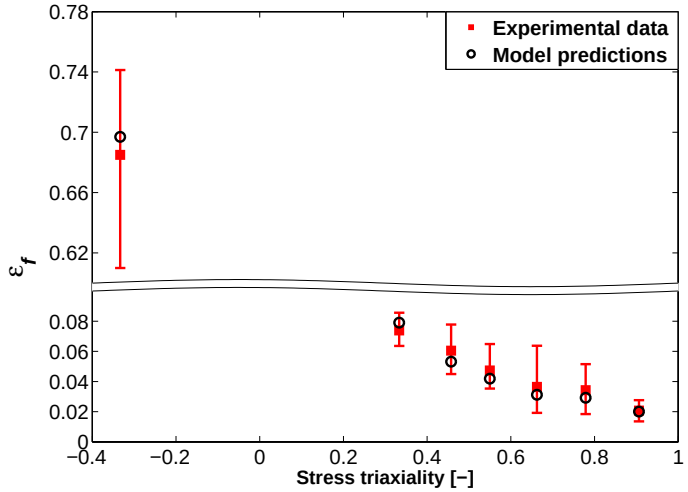

Figure 9: Variation of the experimental and predicted equivalent fracture strain ε_f as a function of the mean stress triaxiality in all the tested specimens (except compression with barreling), involving the error bars corresponding to the experimental data dispersion ; the dots represent the predicted ε_f corresponding to a local MPS = 300MPa and an aspect ratio $A_r = 0.27$.

µm. As previously mentioned, it is assumed that there is statistically always a critical microdefect in the fracture process zone. Therefore, there must be a sufficiently large population of defects inside the fracture process zone. Hence, as the average distance to the crack tip of the fracture process zone is approximated by δ_c, it can be concluded that the microdefects that initiate the cracking process of a macrocrack should be significantly smaller than 1 µm. This argument is also supported by the fact that fractographic analyses of RTM6 specimens have not highlighted the presence of critical defects that would have a detectable size larger than a micron as indicated above. This upper limit of the defect size also justifies the fact that the stress state seen at the RVE level and at the defect scale is actually homogeneous. Moreover, the small size of the defect reinforces the idea that the fracture is initiated in its vicinity when the theoretical strength of RTM6 is reached. Indeed, following the FE analyses presented in this study, the theoretical strength of RTM6 is attained directly at the tip of the defect, that is without the influence of any additional stress concentrator in its neighbourhood. Hence, the probability of finding a zone of pristine material of a size of at least the range of action of the microdefect increases as the size of the defect gets smaller. Now, the exact nature of the defects and whether they are made of nanocracks or simply weaker zones of resin (e.g. with missing cross-links) is still open to discussion.

Still, the arguments based on fracture mechanics do not preclude the existence of defects larger than 1µm from this discussion. Indeed, large defects can obviously have a detrimental influence on the strength of the epoxy resin. Even though no such defect could in general be observed on the fracture surfaces near the initiation site of the fracture, their effect can be examined in two different ways. On the one hand, the combined concentrating effects of a large defect and of a critical microdefect with an aspect ratio $A_r = 0.27$ lead to an earlier fracture as the one predicted by the criterion, which could explain a low fracture strain observed on a few samples (e.g. caused by a poor surface quality). This can be easily linked to the case of the notched specimens. In other words, a population of defects much larger than 1µm would lead to more dispersion in the tests' results, especially with sharp notches. On the other hand, the combined effect of a large defect and a non-critical microdefect can be considered as being equivalent to the stress concentrating effect of a single microdefect properly oriented and with $A_r = 0.27$. The fracture criterion could then be seen as a critical stress attained near a zone whose concentrating effect is equivalent to the one created by a defect with $A_r = 0.27$ and oriented as to maximize the MPS generated.

5. Conclusion

The RTM6 epoxy resin exhibits a much larger ductility in compression than under tensile loadings. Still, in both loading conditions, a brittle fracture mode is observed, indicating a similar underlying failure mechanism. Based on this observation and on other experimental evidences, a new fracture criterion has been proposed based on the assumption of a population of internal microdefects of characteristic aspect ratio A_r acting as stress concentrators. Cracking initiates when the local maximum principal stress at the tip of a defect reaches a critical value.

The main developments and conclusions of the study are the following :

- The criterion has been implemented using a two-scale approach. The experimental tests made on various geometries were simulated in order to determine the stress states at the RVE level at the instant of failure and at the location of the maximum principal stress, this critical stress state was applied to a 3D RVE of RTM6 containing an ellipsoidal defect.
- The identification and the subsequent validation of the model resulted in the determination of the two parameters of the model : the local critical principal stress = 300MPa and the aspect ratio of the critical microdefects = 0.27.
- The failure criterion provides very accurate predictions of the fracture strain in the complete range of loading conditions, encompassing stress states varying between pure compression and moderately high triaxialities in the notched specimen.
- Although the exact nature of the critical defects remains to be determined, they are expected to be of a nanosize, based on the fracture mechanics arguments.

Hence, the richness of this fracture criterion lies in the very good ratio between the number of parameters to be identified (2), the accuracy of the predictions, the versatility in terms of stress states and the connection to physics. The main "cost" is the need to perform FE simulations at two scales. The proposed criterion is believed to remain valid for other epoxy systems, at least on its fundamental principle. Indeed, even though it has only be validated on the RTM6 epoxy resin, other studies report the same failure behaviour and features as the ones exposed in this work but for other epoxy resins (see for example refs [10] and [21]). While the values of the two parameters of the model will differ from a brittle epoxy system to another, the explanation beyond the fracture initiation process is believed to be essentially identical, that is the attainment of a critical stress at the tip of a microdefect. Future works will aim at extending this criterion to precracked specimens and to fatigue conditions, at applying it to other systems and at investigating the nature of the assumed microdefects.

Acknowledgements

The authors acknowledge the financial support of the Interuniversity Attraction Poles Program from the Belgian State through the Belgian Policy agency, contract IAP7/21 INTEMATE. J. Chevalier acknowledges the financial support of the FRIA, Belgium. Computational resources have been provided by the supercomputing facilities of the Université catholique de Louvain (CISM/UCL) and the Consortium des Equipements de Calcul Intensif en Fédération Wallonie Bruxelles (CECI) funded by the Fonds de la Recherche Scientifique de Belgique (FRS-FNRS).

References

[1] A. Puck and H. Schurmann. Failure analysis of {FRP} laminates by means of physically based phenomenological models. *Composites Science and Technology*, 62(1213):1633 – 1662, 2002.

[2] S.T. Pinho, R. Darvizeh, P. Robinson, C. Schuecker, and P.P. Camanho. Material and structural response of polymer-matrix fibre-reinforced composites. *Journal of Composite Materials*, 46(19-20):2313–2341, 2012.

[3] J. Llorca, C. Gonzalez, J.M. Molina-Aldareguia, J. Segurado, R. Seltzer, F. Sket, M. Rodriguez, S. Sadaba, R. Munoz, and L.P. Canal. Multiscale modeling of composite materials: A roadmap towards virtual testing. *Advanced Materials*, 23(44):5130–5147, 2011.

[4] P.A. Carraro and M. Quaresimin. A damage based model for crack initiation in unidirectional composites under multiaxial cyclic loading. *Composites Science and Technology*, 99:154–163, 2014.

[5] W. Van Paepegem, I. De Baere, and J. Degrieck. Modelling the nonlinear shear stress - strain response of glass fibre-reinforced composites. part i: Experimental results. *Composites Science and Technology*, 66(10):1455 – 1464, 2006.

[6] X.P. Morelle, F. Lani, M.A. Melchior, S. Andre, C. Bailly, and T. Pardoen. The elasto-viscoplasticity and fracture behaviour of the rtm6 structural epoxy and impact on the response of woven composites. *ECCM 2012 - Composites at Venice, Proceedings of the 15th European Conference on Composite Materials*, 2012.

[7] X.P. Morelle, J. Chevalier, C. Bailly, T. Pardoen, and F. Lani. Mechanical characterization and modeling of the deformation and failure of the highly cross-linked rtm6 epoxy resin. *International Journal of Plasticity*, submitted.

[8] R.J. Morgan and J.E. O'Neal. The microscopic failure processes and their relation to the structure of amine-cured bisphenol-a-diglycidyl ether epoxies. *Journal of Materials Science*, 12(10):1966–1980, 1977.

[9] R.J. Morgan, E.T. Mones, and W.J. Steele. Tensile deformation and failure processes of amine-cured epoxies. *Polymer*, 23(2):295–305, 1982.

[10] I. Narisawa, T. Murayama, and H. Ogawa. Internal fracture of notched epoxy resins. *Polymer*, 23(2):291–294, 1982.

[11] A.J. Kinloch and R.J. Young. *Fracture Behaviour of Polymers*. Applied Science Publishers, 1983.

[12] L.E. Asp, L.A. Berglund, and R. Talreja. A criterion for crack initiation in glassy polymers subjected to a composite-like stress state. *Composites Science and Technology*, 56(11):1291–1301, 1996.

[13] O.A. Hasan and M.C. Boyce. Constitutive model for the nonlinear viscoelastic viscoplastic behavior of glassy polymers. *Polymer Engineering and Science*, 35(4):331–344, 1995.

[14] O. Sindt, J. Perez, and J.F. Gerard. Molecular architecture-mechanical behaviour relationships in epoxy networks. *Polymer*, 37(14):2989 – 2997, 1996.

[15] T. Hobbiebrunken, M. Hojo, B. Fiedler, M. Tanaka, S. Ochiai, and K. Schulte. Thermomechanical analysis of micromechanical formation of residual stresses and initial matrix failure in cfrp. *JSME International Journal, Series A: Solid Mechanics and Material Engineering*, 47(3):349–356, 2004.

[16] R. Gerlach, C.R. Siviour, N. Petrinic, and J. Wiegand. Experimental characterisation and constitutive modelling of rtm-6 resin under impact loading. *Polymer*, 49(11):2728–2737, 2008.

[17] A.E. Mayr, W.D. Cook, and G.H. Edward. Yielding behaviour in model epoxy thermosets - i. effect of strain rate and composition. *Polymer*, 39(16):3719–3724, 1998.

[18] W.D. Cook, A.E. Mayr, and G.H. Edward. Yielding behaviour in model epoxy thermosets - ii. temperature dependence. *Polymer*, 39(16):3725–3733, 1998.

[19] T. Gomez-del Rio and J. Rodriguez. Compression yielding of epoxy: Strain rate and temperature effect. *Materials and Design*, 35:369–373, 2012.

[20] X. Poulain, A.A. Benzerga, and R.K. Goldberg. Finite-strain elasto-viscoplastic behavior of an epoxy resin: Experiments and modeling in the glassy regime. *International Journal of Plasticity*, 62:138–161, 2014.

[21] B. Fiedler, M. Hojo, S. Ochiai, K. Schulte, and M. Ando. Failure behavior of an epoxy matrix under different kinds of static loading. *Composites Science and Technology*, 61(11):1615–1624, 2001.

[22] Dominique Leguillon. Strength or toughness? a criterion for crack onset at a notch. *European Journal of Mechanics - A/Solids*, 21(1):61 – 72, 2002.

[23] D. Taylor. Applications of the theory of critical distances in failure analysis. *Engineering Failure Analysis*, 18(2):543–549, 2011.

[24] H. Askes, P. Livieri, L. Susmel, D. Taylor, and R. Tovo. Intrinsic material length, theory of critical distances and gradient mechanics: Analogies and differences in processing lineara-elastic crack tip stress fields. *Fatigue and Fracture of Engineering Materials and Structures*, 36(1):39–55, 2013.

[25] A.J. Kinloch, S.J. Shaw, and D.L. Hunston. Deformation and fracture behaviour of a rubber-toughened epoxy: 2. failure criteria. *Polymer*, 24(10):1355–1363, 1983.

[26] P.H. Martiny, F. Lani, A.J. Kinloch, and T. Pardoen. A maximum stress at a distance criterion for the prediction of crack propagation in adhesively-bonded joints. *Engineering Fracture Mechanics*, 97(1):105–135, 2012.

[27] J. Li and X.B. Zhang. A criterion study for non-singular stress concentrations in brittle or quasi-brittle materials. *Engineering Fracture Mechanics*, 73(4):505–523, 2006.

[28] X.B. Zhang and J. Li. A failure criterion for brittle and quasi-brittle materials under any level of stress concentration. *Engineering Fracture Mechanics*, 75(17):4925–4932, 2008.

[29] E.Z. Wang and N.G. Shrive. On the griffith criteria for brittle fracture in compression. *Engineering Fracture Mechanics*, 46(1):15–26, 1993.

[30] E.Z. Wang and N.G. Shrive. Brittle fracture in compression: Mechanisms, models and criteria. *Engineering Fracture Mechanics*, 52(6):1107–1126, 1995.

[31] E.Z. Wang and N.G. Shrive. A 3-d ellipsoidal flaw model for brittle fracture in compression. *International Journal of Solids and Structures*, 36(27):4089–4109, 1999.

[32] A. A. Griffith. The phenomena of rupture and flow in solids. *Philosophical Transactions of the Royal Society of London A: Mathematical, Physical and Engineering Sciences*, 221(582-593):163–198, 1921.

[33] ABAQUS 6.12/Standard Users Manual. Hibbit, Karlsson and Sorensen Inc., Pawtucket, RI, 2012.

[34] A.C. Steenbrink, E. Van Der Giessen, and P.D. Wu. Void growth in glassy polymers. *Journal of the Mechanics and Physics of Solids*, 45(3):405 – 437, 1997.

[35] D. Hull. The effect of mixed mode i/iii on crack evolution in brittle solids. *International Journal of Fracture*, 70(1):59–79, 1995.

[36] T. Hobbiebrunken, B. Fiedler, M. Hojo, and M. Tanaka. Experimental determination of the true epoxy resin strength using micro-scaled specimens. *Composites Part A: Applied Science and Manufacturing*, 38(3):814–818, 2007.

[37] S. N. Zhurkov and V. E. Korsukov. Atomic mechanism of fracture of solid polymers. *Journal of Polymer Science: Polymer Physics Edition*, 12(2):385–398, 1974.

[38] G. J. Lake and A. G. Thomas. The strength of highly elastic materials. *Proceedings of the Royal Society of London A: Mathematical, Physical and Engineering Sciences*, 300(1460):108–119, 1967.

[39] A. Kelly. *Strong solids*. Oxford : Clarendon, first edition, 1966.

[40] T. L. Anderson. *Fracture mechanics, Fundamentals and Applications*. CRC Press, Boca Raton (US-FL), third edition, 2005.